SUSTAINABLE WATER MANAGEMENT AND RIVER DEVELOPMENT

VOLUME II

Editors: Lin Luo
Shaw Lei Yu

PROCEEDINGS OF THE 5TH INTERNATIONAL CONFERENCE ON URBAN WATERSHED MANAGEMENT & MOUNTAIN RIVER PROTECTION AND DEVELOPMENT

APRIL 3-5. 2007
CHENGDU, CHINA

SICHUAN UNIVERSITY PRESS

Contents

Theme C Hydraulics and River Dynamics

Theme D River Protection and Development

THE FLOW CHARACTERISTIC OF CULVERT AND SLUICE AND ITS INFLUENCE ON THE ONCEMELANIA DIFFUSION

Guoyu Jin, Damei Li, Xuan Ban

School of Water Resource and Hydropower, Wuhan University, Wuhan, China, 430072

E-mail: jinguoyulm@sina.com

ABSTRACT

Schistosomiasis is the harmful verminoses along the Yangtze River. Oncemelania is middle-parasitizeder of Schistosomes. So controlling oncemelania diffusion is the most important and effective way to prevent the spread of schistosomiasis. Irrigation canal, culvert and sluice between agricultural fields are important water conservancy facilities of agricultural irrigation; They are also main channels which oncemelania can diffuse though. The article mainly introduces the measurement of the velocity distribution by ADV, standard k-epsilon and hybrid finite analytic method (HFAM) numerical modeling. Lastly demonstrating the cause why the purpose of holding oncemelania back cannot be achieved only by culvert and sluice, and on the contrary, a little part of oncemelania may breed and diffusion locally by two ways of experiment and numerical stimulating.

KEYWORDS

Oncemelania, Culvert and Sluice, ADV, HFAM, Flow field

1 INTRODUCTION

Schistosomiasis is the major parasitic disease in China and it is mostly found in the areas along the Yangtze River. Oncemelania is the key middle agent who carries and spreads schistosomiasis. Controlling oncemelania diffusion is the most effective way to control schistosomiasis. Oncomelania belongs to amphibious fresh water snail, its child must live in waters. The oncemelania diffuses widely due to many hydraulic engineering, such as intaking, irrigation, diversion, electricity generation, navigation, ects, which brings the hard work of destroying oncemelania.

Culvert and sluice is the common water resource facility and frequently used in irrigation areas, it is also the main diffusion gate of oncemelania. With the construction of the few decade infrastructures, the nearly complete Yangtze valley irrigation and drainage system has been built. However, ditches crisscross, rivers connect ditches, ditches connect stanks, stanks connects fields, fields connects villages, which provides favorable conditions for oncemelania's diffusion in all directions. Thus, the research of culvert and sluice's flow characteristics and its impact on oncemelania's diffusion is very necessary and important for reducing the cost of schistosomiasis prevention and cure, protecting security of human and livestock and improving development of industries and agricultures in pestilence areas.

2 EXPERIMENT DEVICES AND RESULTS

The flow characteristic of culvert is similar with that of the broad-crested weir, thus, instead of culvert and sluice, the broad-crested weir is used to simulate the flow characteristics. The experiment equipments are illustrated as Figure 1 which contain a culvert and sluice (broad-crested weir without ridge), 1.5 m from the downstream valve, and a channel ($5.6 \times 0.5 \times 0.6$ m^3). Organic glass is affixed inside of the channel to get the accordant viscosity. In order to stabilize inlet flow rate and smooth the flow, the flow-steadying grid is equipped at the channel inlet. An end gate is utilized to control downstream water level. The depth of water is 0.5 m, keeping the temperature 28℃ and the flow rate 0.0359 m^3/s. MicroADV of Sontek is adopt as velometer, its probe can move in all directions by controlling handles. The measurement area is located at a plane of 0.2 m deep of the water.

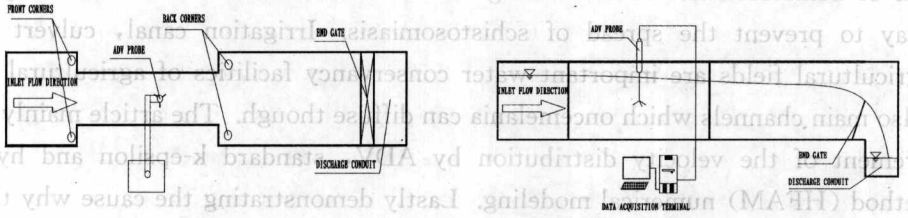

(a)Top view (b)Side view

Figure 1 Experiment device sketch

At the beginning of experiment, the valve is adjusted to keep downstream water level 0.5 m. ADV starts working as soon as the flow gets smooth. The distribution of velocity and flow field by ADV is illustrated as Figure 2, Figure 3, respectively. At the end of experiment, oncemelania is released at the inlet section to observe its sedimentation and diffusion. The result shows that only about 10% deposits at the four corners around culvert and sluice, and the other 90% oncemelania diffuses along the main stream. All these facts indicate that culvert and sluice cannot prevent the oncemelania's diffusion effectively. The sedimentary spots are illustrated as Figure 4 from the figure, In comparison with a little oncemelania at the corners in front of the culvert and sluice, much oncemelania sinks at the back corners.

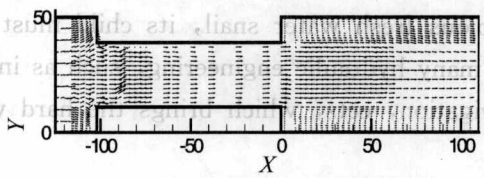

Figure 2 Experiment velocity distribution sketch

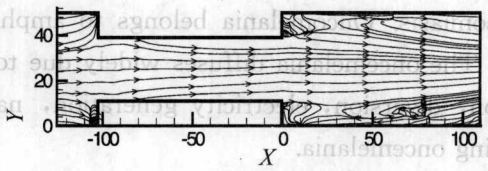

Figure 3 Streamline sketch

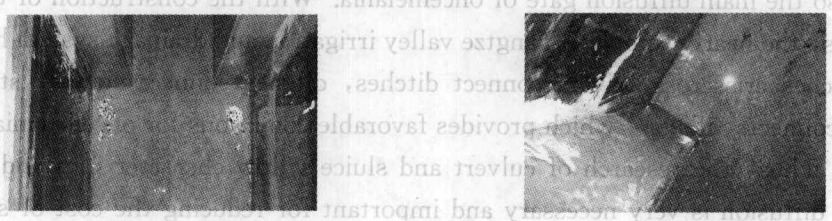

(a) Oncemelania at back corners (b) Oncemelania at front corner

Figure 4 Distribution of oncemelania sketch

3 NUMERICAL STIMULATION OF FLOW FIELD

In order to find out the characteristics of the ecological flow field, Using the close Navier-Stokes equations, the standard κ-ε double equations model, SIMPLE algorithm, and preferred turbulence model coefficients, along with the corresponding hybrid finite analytic method (HFAM), numerically simulating the flow field in the three-dimensional rectangular channel (Figure 2). The following is the κ-ε double equations model:

3.1 Equation of Continuity

$$\frac{\partial u}{\partial x}+\frac{\partial v}{\partial y}+\frac{\partial w}{\partial z}=0 \tag{1}$$

3.2 Momentum Equation

$$\begin{aligned}&\frac{\partial u}{\partial t}+\left(u-2\frac{\partial v_t}{\partial x}\right)\frac{\partial u}{\partial x}+\left(v-\frac{\partial v_t}{\partial y}\right)\frac{\partial u}{\partial y}+\left(w-\frac{\partial v_t}{\partial z}\right)\frac{\partial u}{\partial z}=-\frac{1}{\rho}\frac{\partial p}{\partial x}-\frac{2}{3}\frac{\partial k}{\partial x}\\&+(v+v_t)\frac{\partial^2 u}{\partial x^2}+(v+v_t)\frac{\partial^2 u}{\partial y^2}+(v+v_t)\frac{\partial^2 u}{\partial z^2}+\frac{\partial v_t}{\partial y}\frac{\partial v}{\partial x}+\frac{\partial v_t}{\partial z}\frac{\partial w}{\partial x}\end{aligned} \tag{2}$$

$$\begin{aligned}&\frac{\partial v}{\partial t}+\left(u-\frac{\partial v_t}{\partial x}\right)\frac{\partial v}{\partial x}+\left(v-2\frac{\partial v_t}{\partial y}\right)\frac{\partial v}{\partial y}+\left(w-\frac{\partial v_t}{\partial z}\right)\frac{\partial v}{\partial z}=-\frac{1}{\rho}\frac{\partial p}{\partial y}-\frac{2}{3}\frac{\partial k}{\partial y}\\&+(v+v_t)\frac{\partial^2 v}{\partial x^2}+(v+v_t)\frac{\partial^2 v}{\partial y^2}+(v+v_t)\frac{\partial^2 v}{\partial z^2}+\frac{\partial v_t}{\partial x}\frac{\partial u}{\partial y}+\frac{\partial v_t}{\partial z}\frac{\partial w}{\partial y}\end{aligned} \tag{3}$$

$$\begin{aligned}&\frac{\partial w}{\partial t}+\left(u-\frac{\partial v_t}{\partial x}\right)\frac{\partial w}{\partial x}+\left(v-\frac{\partial v_t}{\partial y}\right)\frac{\partial w}{\partial y}+\left(w-2\frac{\partial v_t}{\partial z}\right)\frac{\partial w}{\partial z}=-\frac{1}{\rho}\frac{\partial p}{\partial z}-\frac{2}{3}\frac{\partial k}{\partial z}\\&+(v+v_t)\frac{\partial^2 w}{\partial x^2}+(v+v_t)\frac{\partial^2 w}{\partial y^2}+(v+v_t)\frac{\partial^2 w}{\partial z^2}+\frac{\partial v_t}{\partial x}\frac{\partial u}{\partial z}+\frac{\partial v_t}{\partial y}\frac{\partial v}{\partial z}\end{aligned} \tag{4}$$

3.3 Turbulence k Equation

$$\begin{aligned}&\frac{\partial k}{\partial t}+\left(u-\frac{1}{\sigma_k}\frac{\partial v_t}{\partial x}\right)\frac{\partial k}{\partial x}+\left(v-\frac{1}{\sigma_k}\frac{\partial v_t}{\partial y}\right)\frac{\partial k}{\partial y}+\left(w-\frac{1}{\sigma_k}\frac{\partial v_t}{\partial z}\right)\frac{\partial k}{\partial z}\\&=\left(v+\frac{v_t}{\sigma_k}\right)\left(\frac{\partial^2 k}{\partial x^2}+\frac{\partial^2 k}{\partial y^2}+\frac{\partial^2 k}{\partial z^2}\right)+P_k-\varepsilon\end{aligned} \tag{5}$$

3.4 Turbulence Dissipation ε Equation

$$\begin{aligned}&\frac{\partial \varepsilon}{\partial t}+\left(u-\frac{1}{\sigma_\varepsilon}\frac{\partial v_t}{\partial x}\right)\frac{\partial \varepsilon}{\partial x}+\left(v-\frac{1}{\sigma_\varepsilon}\frac{\partial v_t}{\partial y}\right)\frac{\partial \varepsilon}{\partial y}+\left(w-\frac{1}{\sigma_\varepsilon}\frac{\partial v_t}{\partial z}\right)\frac{\partial \varepsilon}{\partial z}\\&=\left(v+\frac{v_t}{\sigma_\varepsilon}\right)\left(\frac{\partial^2 \varepsilon}{\partial x^2}+\frac{\partial^2 \varepsilon}{\partial y^2}+\frac{\partial^2 \varepsilon}{\partial z^2}\right)+(C_1P_k-C_{2\varepsilon})\frac{\varepsilon}{k}\end{aligned} \tag{6}$$

where $v_t=C_\mu\dfrac{k^2}{\varepsilon}$

$$P_k=v_t\left[2\left(\frac{\partial u}{\partial x}\right)^2+2\left(\frac{\partial v}{\partial y}\right)^2+2\left(\frac{\partial w}{\partial z}\right)^2+\left(\frac{\partial v}{\partial x}+\frac{\partial u}{\partial y}\right)^2+\left(\frac{\partial w}{\partial y}+\frac{\partial v}{\partial z}\right)^2+\left(\frac{\partial u}{\partial z}+\frac{\partial w}{\partial x}\right)^2\right]$$

3.5 Model Constant

$$C_\mu = 0.09,\ C_1 = 1.44,\ C_2 = 1.92,\ \sigma_k = 1.0,\ \sigma_\varepsilon = 1.3$$

3.6 Boundary Condition

① inlet

$$u = u_0 = 0.3\ \text{m/s},\ v = w = 0,\ k_0 = 0.001u_0^2,\ \varepsilon = \frac{k_0^{1/2}}{0.06D}$$

② outlet

$$\frac{\partial u}{\partial x} = \frac{\partial v}{\partial x} = \frac{\partial w}{\partial x} = \frac{\partial k}{\partial x} = \frac{\partial \varepsilon}{\partial x} = 0$$

③ free surface

VOF model is adopted, that is, the water and air are two phases, respectively. Wall function is used in the other boundaries.

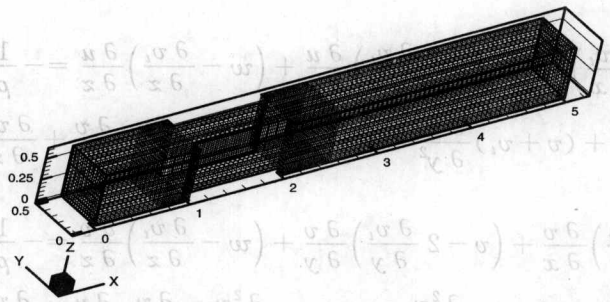

Figure 5 Calculating mesh sketch

4 DISCUSSION

Figure 5 shows the calculating mesh whereas Figures 6—9 present the calculated streamlines on each cross-section. Since the study is mainly concerned with the oncemelania's diffusion along the flow, the flow structure of X-Y sections and only sections vertical to axis Z with $z = 0.01$ m, $z = 0.2$ m, $z = 0.4$ m and $y = 0.25$ m are selected to facilitate the observation of changes in the three-dimensional flow field. The study has indicated:

(1) Generally speaking, the whole flow structure is symmetrical on the cross-sections with $z = 0$, namely, it is symmetrical with respect to its left and right parts. And each section is similar basically. (except the section with $z = 0.4$ m due to the influence of air)

(2) Due to the limitation of experiment conditions as the following: The model shape cannot be exactly symmetrical compared with numerical stimulation model; The experiment flow cannot be absolute uniform flow; The back flow from downstream caused by short distance between the end gate and vortex influences the formation and stability of vortex; also, the noise and particle concentration have certain influence on measurement precision, calculation differs with experiment. However, the comparison of the two results of Figure 2 and Figure 3 shows that the structure, changing trend and the position of vortex are accordant. The numerical calculation results can be accepted.

(3) The comparison demonstrated that, on the one hand, due to the high speed of mainstream in the culvert and sluice, the majority of oncemelania diffuses along the mainstream,

on the other hand, at the adjacent place between main stream and vortex, a little oncemelania is strolled and deposits at the four corners around culvert and sluice, Furthermore, more oncemelania will diffuse along the downstream, and correspondingly, less oncemelania will deposit with the increase of inlet velocity. General speaking, culvert and sluice cannot prevent oncemelania's diffusion effectively.

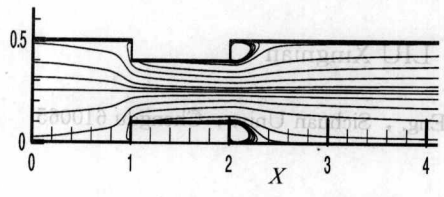

Figure 6 Streamline at section $z=0.01$ m

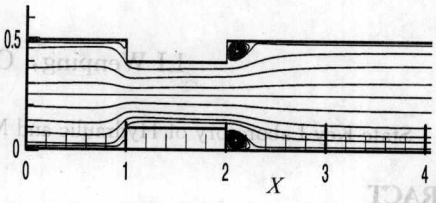

Figure 7 Streamline at section $z=0.2$ m

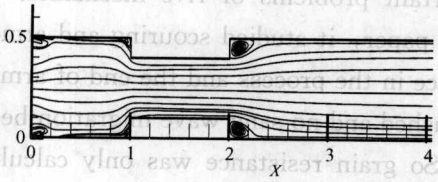

Figure 8 Streamline at section $z=0.4$ m

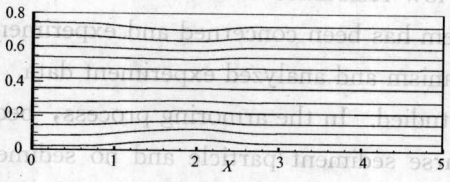

Figure 9 Streamline at section $y=0.25$ m

5 CONCLUSIONS

The following conclusions can be drawn from above comparisons and analyses between experiments and numerical stimulations:

(1) The fields' ditch is the main diffusion channel of oncemelania and schistosomiasis in irrigation areas;

(2) On base of the experiment and calculation, the culvert and sluice does not have the function of preventing oncemelania;

(3) The place around culvert is easy for oncemelania to sink and should be paid attention to become the new breed site, thus, it's the most important site for destroying oncemelania;

(4) The research could provide scientific basis for schistosomiasis prevention and avoid putting in much drug which causes environmental pollutions and economic damages;

(5) Other methods should be adopted to control the oncemelania's diffusion in irrigation areas, such as water-intake without oncemelania.

ACKNOWLEDGEMENTS

This work is supported by national natural science foundation of China (NSFC) (No. 50179027)

REFERENCES

LiDamei. Study of water intakes for Oncemelania control based on information of Oncemelania behavior and CFD results [J]. Science in china, 2001, Vol. 10, 22−26.

Li Wei. Hybrid finite analytic solution of viscid fluid [M]. Science press, 2000, 79−107.

Liang Zaichao. Engineering turbulent [M]. Huazhong university of science and technology press, 1994, 85−98.

Liu Dayou. Two-phase flow dynamics [M]. High education press, 1993, 20−86.

Rodi, W. Turbulence Models and their Application in Hydraulics- A state of Art Review [M]. IAHR Monograph, 3rd edition, Balkema, Rotterdam, 1993.

Tao Wenquan. Numerical heat transfer [M]. Xi'an university Jiao Tong press, 1988, 203−224.

RESISTANCE STUDY ON SCOURING AND ARMORING OF FLUME EXPERIMENT WITH WIDE SIZE-DISTRIBUTION BY CLEAR WATER*

LI Wenping, CAO Shuyou, LIU Xingnian

State Key Laboratory of Hydraulic and Mountain River Eng., Sichuan Univ., Chengdu 610065

ABSTRACT

Flow resistance of moveable bed is one of important problems of rive mechanics. This problem has been concerned and experimented. In this paper, it studied scouring and armoring mechanism and analyzed experiment data. The resistance in the process and the end of armoring was studied. In the armoring process, bed load was pushed and no sand wave migration because of coarse sediment particle and no sediment supply. So grain resistance was only calculated. When river-bed has been scoured until armoring stable structure was formed. River-bed surface would be in regime of plane bed and no bed load. Fixed bed resistance is the most primary after armoring stabilization. By theoretically analyzing, resistance low in the process and the end of armoring was established. Verified by using of experiment data, the result showed that experiment data was adjacent to measured values.

* Supported by National Key Basic Research and Development Program of China. (973 Program) (2003CB415202)

STUDY ON THE RELATIONSHIP BETWEEN THE HEIGHT OF THE FIRST STEP AND HYDRAULIC PARAMETERS OF THE FLARING GATE PIER*

Hu Yao-hua, Wu Chao, Wang Bo, Mo Zheng-yu

State Key Lab. of Hydraulics and Mountain River Engineering, Sichuan Univ., Chengdu 610065, China

ABSTRACT

As the bottom of X-shaped flaring gate piers outlet is flared and the first step is higher than others, the water flow over the steps forms a nappe and an air cavity exists between the nappe and the step face. As a result, there is a non-water region behind the flaring gate piers, connecting to the atmosphere. Air is entrained to this region, and the water over the step face is aerated. This paper presents the relationship existing the hydraulic parameters of both the first step and flaring gate piers, and the formula for the cavity length. The calculated results agree well with the data of both the numerical simulation and model. The finding indicate that the height difference between the first and second steps is the main factor influencing the cavity, and more attention should be placed on the role of the first step.

KEYWORDS

flaring gate pier, the height of the first step, aerated cavity, hydraulic parameters

1 INTRODUCION

Flood discharge and the energy dissipation are the important topic in the dam design. Stepped spillways are applied widely and used in plenty of projects at home and abroad.

The energy dissipation of stepped spillways relates to the discharge, dam height, step height and the chute slope. At low heads and small unit discharges, the water flow cascades over the steps and is aerated, dissipating energy. However, the flow depth over the step face is increased, the condition for the bottom aeration is absent, and the stepped spillways may become prone to cavitation damage at high heads and large unit discharges. Thus, the unit discharge of stepped spillways is limited to 30 m^3/s. In order to increasing the unit discharge of stepped spillways, a new dissipator, flaring gate pier (FGP) is proposed, which is made by flaring the pier rear. For the construction progress, the unit dissipation system of FGP and stepped spillways appears with the merits of FGP and stepped spillways and is used widely in practice.

X-shaped FGP is an advanced one with a widened bottom. When the discharge is not large, the flow mainly passes through the bottom of chamber, forming a thin jet, which can meet the demand of small larges that often take place. The first step height is increased due to the large flow over step face. When the first step is higher than others, an air cavity is formed behind FGP

* Project supported by the National Natural Science Foundation of China (Grant No. 50479061)

and the flow is aerated. In Suofengying hydro plant, the actual unit discharge exceeds 30 m^2/s, but there is no cavitation damage to the steps.

The steps are prevented from cavitation damage, because the large region without water over the step face makes the ventilation from both sides of FGP to the jet bottom possible. There is no report about the calculation of the air cavity size and the analyses of the influencing factors. In this paper, the relationship of hydraulic parameters at the variation of the first step height is investigated by theoretical analysis and numerical simulation.

2 THEORETICAL ANALYSIS OF THE RELATIONSHIP BETWEEN THE FIRST STEP HEIGHT AND HYDRAULIC PARAMETERS OF FGP

The hypothesis of jet trajectory is employed. The lower jet separates from the spillway, resulting in an air cavity between the lower jet and the step face, and the jet falls on the step at the end. The diagrammatical sketch of nappe calculation is shown in Figure 1.

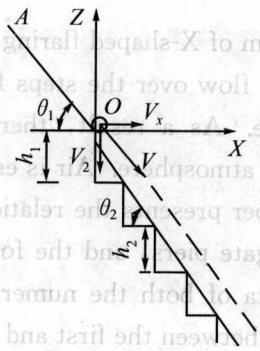

Figure 1 Diagrammatical sketch of nappe calculation

The weir AO is connected to a stepped surface, and the slope angle of weir end is θ_1. The first step height is h_1; the others are h_2, the step width is b and the slope angle of step is θ_2. In the coordinates, the initial point O is located at the junction of the weir and steps. The characteristic number of cavity n is defined by $n=x/b$. On the plane of XOZ, the velocity of nappe at the initial point is denoted by v. Without consideration of air resistance, the equation for the trajectory of nappe is expressed by

$$z = -x\tan\theta_1 - \frac{gx^2}{2V^2}(1+\tan^2\theta_1) \tag{1}$$

The equation for the grade line of step is expressed by

$$z = -x\tan\theta_2 - (h_1 - h_2) \tag{2}$$

The x-coordinate of intersection can be obtained from Eqs. (1) and (2)

$$x = \frac{V^2}{g}\left[\frac{(\tan\theta_2 - \tan\theta_1) + \sqrt{(\tan\theta_2 - \tan\theta_1)^2 + 2g(h_1 - h_2)(1+\tan^2\theta_1)/V^2}}{1+\tan^2\theta_1}\right] \tag{3}$$

Liu et al. presented that there was a difference between the result calculated by Eq. (3) and that from prototype observation; and the probable error might be up to 30% or more. Li reported that the horizontal component of a trajectory jet calculated was 1.2—1.6 times of the factual one, i.e. the true value was lower as compared with that computed by Eq. (3). Thus, a coefficient less than 1 should be offered to Eq. (3). Introducing the elevation difference between the crest and the chamber outlet h and the crest head h', the following equation can be given by dividing the step width b

$$n = 2K\varphi\frac{(h+h')}{b}\left\{\frac{(\tan\theta_2 - \tan\theta_1) + \sqrt{(\tan\theta_2 - \tan\theta_1)^2 + (h_1 - h_2)(1+\tan^2\theta_1)/[\varphi(h+h')]}}{1+\tan^2\theta_1}\right\} \tag{4}$$

where K is the coefficient of air resistance, φ denotes the transformation coefficient of potential and pressure energy to kinetic energy from the crest to the point O, $\varphi=\dfrac{v^2}{2g\ (h+h')}$, which can be obtained by model experiment or numerical simulation.

Eq. (4) indicates that the main factors influencing the cavity formation are the elevation difference between the crest and chamber outlet, the first height and second steps, the weir end slope, the step slope. The investigation on these relationships helps to choose the size of step, design the slope of weir end, control the aerated cavity and utilize the step efficiently.

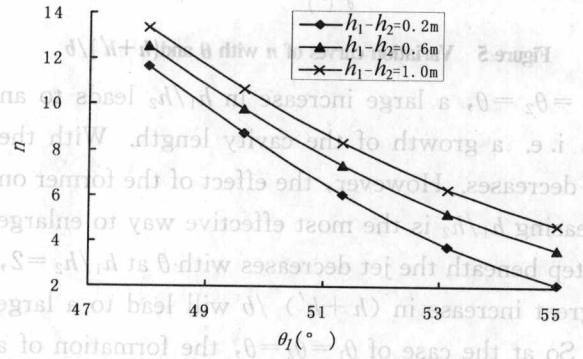

Figure 2 Variation curves of n with θ_1 and(h_1-h_2)

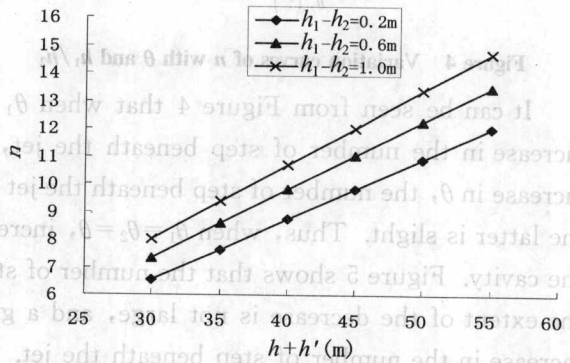

Figure 3 Variation curves of n with($h+h'$) and(h_1-h_2)

If $\theta_1<\theta_2$, Figure 2 presents the variation of the number of steps n beneath the lower jet with the weir slope angle θ_1 at different h_1-h_2 and $\theta_2=55.01°$, $h+h'=40$ m, $b=0.84$ m. It can be seen that the value of n, i. e. the length of cavity, increases with decreasing the weir slope angle θ_1 or increasing the value of $\tan\theta_2-\tan\theta_1$. When the value of h_1-h_2 keeps constant, a little increase in $\tan\theta_2-\tan\theta_1$ can lead to a lengthened cavity. When the weir slope angle reduces, the influence of h_1-h_2 on the cavity size becomes light. Figure 3 presents the variation of the number of steps n beneath the lower jet with $h+h'$ at different h_1-h_2 and $\theta_1=49.63°$, $\theta_2=55.01°$, $b=0.84$ m. It shows a basically linear change of the cavity length with $h+h'$. Thus when $\tan\theta_2-\tan\theta_1>0$ and $h_1-h_2>0$, the effects of $h+h'$ and h_1-h_2 on the cavity is not obvious, the cavity length primarily depends on $\tan\theta_2-\tan\theta_1$, and a little change of $\tan\theta_2-\tan\theta_1$ results in a visible one of the cavity length.

If $\theta_1=\theta_2=\theta$, Eq. (4) yields

$$n=\varphi_1\cdot\sqrt{\frac{h_1}{h_2}-1}\cdot\sqrt{\frac{2(h+h')}{b}}\cdot\sqrt{\sin 2\theta} \tag{5}$$

where $\varphi_1=K\cdot\sqrt{\varphi}$, in this case, n is a function of h_1/h_2, $(h+h')/b$, θ.

Based on the FGP existing and under construction, the range of the elevation difference between the crest and chamber outlet is 15 m~30 m, the crest head is 10 m~30 m, and the step width is below 1 m. FGP is equipped with the stepped spillway, with a step slope of 1 : 0.70 and a weir slope less than 1 : 0.75. The relationship curves of n, h_1/h_2, $(h+h')/b$, θ can be obtained from Eq. (5), shown in Figures 4 and 5.

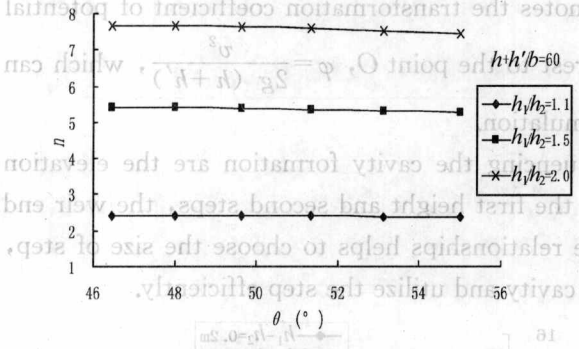

Figure 4 Variation curves of n with θ and h_1/h_2

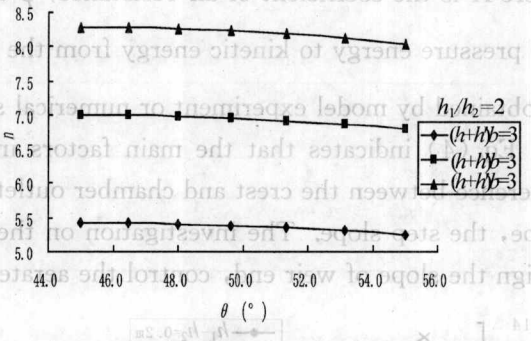

Figure 5 Variation curves of n with θ and $(h+h')/b$

It can be seen from Figure 4 that when $\theta_1=\theta_2=\theta$, a large increase in h_1/h_2 leads to an increase in the number of step beneath the jet, i. e. a growth of the cavity length. With the increase in θ, the number of step beneath the jet decreases. However, the effect of the former on the latter is slight. Thus, when $\theta_1=\theta_2=\theta$, increasing h_1/h_2 is the most effective way to enlarge the cavity. Figure 5 shows that the number of step beneath the jet decreases with θ at $h_1/h_2=2$, the extent of the decrease is not large, and a great increase in $(h+h')/b$ will lead to a large increase in the number of step beneath the jet. So at the case of $\theta_1=\theta_2=\theta$, the formation of a cavity beneath the jet needs the first step higher than others. When the height of the fist step is fixed, the variation of the weir slope does not affect the cavity heavily. Thus, in the design phase, the height of the first step and the slope angle can be determined according to the number of step beneath the jet needed.

3 NUMERICAL SIMULATION OF THE RELATIONSHIP BETWEEN THE FIRST STEP HEIGHT AND HYDRAULIC PARAMETERS OF FGP

There are five gates in the Suofengying hydro plant. The head of the possible maximum discharge is 105.37 m and the unit discharge at the design flooding is 179 m^3/s. The design scheme of Suofengying hydro plant is following: $\theta_1=49.63°$, $h=21.24$ m, $h'=37.97$ m, $h_1=1.46$ m, $h_2=1.20$ m, $h_1-h_2=0.26$ m, $\theta_2=55.01°$, $b=0.84$ m. The experimental result indicates that there are 6 − 8 steps beneath the jet. The number of step beneath the jet calculated by Eq. (4) is $n=8.72$, which agrees well with the model data.

In this paper, the FLUENT CFD was used to simulate the three-dimensional flow field of the united dissipation of FGPs, a stepped spillway and a stilling basin. The VOF method was adopted to track the free surface. The $k-\varepsilon$ model turbulence models was used.

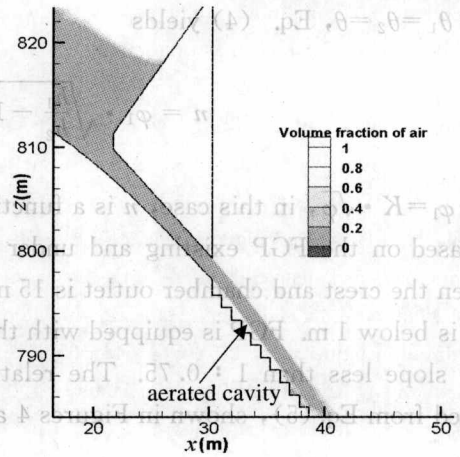

Figure 6 Cavity on the downstream of flaring gate piers

Figure 6 shows the air cavity behind the FGP at $h_1=1.46$ m. It can be seen that there is a non-water region occupying the fist six steps. The numbers of step beneath the jet simulated by FLUENT and calculated by Eq. (4) at different height of the first step are listed in Table 1. It

can be concluded that the simulation result agrees well with the data of calculation and model.

Table 1 Dependence of cavity on different heights of the first step

h_1 (m)	h_1-h_2 (m)	n	
		simulation result	calculation result
1.76	0.56	$n=9-10$	$n=9.45$
1.60	0.4	$n=8-9$	$n=9.08$
1.46	0.26	$n=6-7$	$n=8.72$

4 CONCLUSIONS

X-shaped FGP is an improved type. The lower part of the gate exit is widen by X-shaped FGP followed by the stepped spillway, so the discharge passed the steps is increased. The first step is higher than the others. The cavity is occurred at back of the FGP, so flow becomes water-air two phase at the face of steps.

The paper analyses the size of cavity and the affect factors by numerical stimulation. The formula to calculate the size of cavity is yielded. The paper studies the affection to cavity where the slope of end of the weir does not coincide with the slope of the steps, and the affections of both and the difference of the first steps and the second steps. The paper proposes the effect of the first steps should be considered fully at design where the slope of end of the weir coincides with the slope of the steps.

REFERENCES

Gan Huiqi, Ling Xianzong, Li Xia. 1999. Research and test for united dissipation of energy of the wide tail pier-bucket type stilling pool of the Bajiangkou hydropower station [J]. GX water resources & hydropower engineering, (2): 19–21.

George C Christodoulou. 2006. Energy dissipation on stepped spillways [J]. Journal of Hydraulic Engineering, 132 (8): 850–853.

Hipt C W, Nichols B D. 1981. Volume of Fluid (VOF) method for the dynamics of boundaries [J]. Journal of Computational physics, 39 (1): 201–225.

Liang Zongxiang, Yin Jinbu, Liu Hansheng, et al. 2003. Experimental study on united dissipater with stepped spillway dam surface and flaring gate piers [J]. Journal of Yangtze river scientific research, 20 (6): 3–5.

Li Chongzhi. 1963. A study of trajectory of the high velocity jet from flip bucket [J]. Journal of Hydraulic Engineering, (2): 25–32.

Liu Xunlie, Chang Wenzhou. 1982. Effect of air resistance to a trajectory jet [J]. Journal of Tianjin University, 15 (2): 67–77.

Lin Keji, Han Li, Deng Yiguo. 2002. Study and application of the combined energy dissipator of overflow dam flaring piers and stepped dam face in the Dachaoshan hydropower plant [J]. Yunnan Water Power, 18 (4): 6–15.

Michael Ptister, Willi H Hager, Hans-Enwin Minor. 1993. Bottom aeration of stepped spillways [J]. Journal of Hydraulic Engineering, 119 (5): 644–650.

Nan Xiaohong, Liang Zongxiang, Liu Hansheng. 2003. New type of flaring pier for improving energy dissipation of stepped surface overflow dam [J]. Journal of Hydraulic Engineering, 34 (8): 49–57.

Rong Quanhua, Xu Muyun. 1996. Research on the new type energy dissipater with flared gate piers of Yantan hydropower station [J]. Hong He Shui, 15 (2): 4–6.

Yang Shoulong. 2004. New techniques and its functions for release works in Fujian province [J]. Journal of Hydroelectric Engineering, 23 (1): 84–90.

STUDY ON AERATOR FORM OF FREE-FLOW SPILLWAY TUNNEL WITH HIGH HEAD

Haiyun Wang[1], Guangqing Dai[2], Chao Liu[3], Qing Yang[4] and Yangsong Yin[5]

[1] State Key Lab. of Hydraulics and Mountain River Engineering, Sichuan Univ., Chengdu 610065, China. E-mail: whyskhl@126.com

[2] State Key Laboratory of Hydraulics and Mountain River Engineering, Sichuan Univ., Chengdu 610065, China. E-mail: daiqq01@126.com

[3] State Key Laboratory of Hydraulics and Mountain River Engineering, Sichuan Univ., Chengdu 610065, China. E-mail: liuchaogood@sohu.com

[4] State Key Laboratory of Hydraulics and Mountain River Engineering, Sichuan Univ., Chengdu 610065, China. E-mail: youngking411@126.com

[5] State Key Laboratory of Hydraulics and Mountain River Engineering, Sichuan Univ., Chengdu 610065, China. E-mail: yinyangsong@126.com

ABSTRACT

For behind concave reach side-walls of Vertical-Bend free flow spillway tunnel, acted by centrifugal force and pressure characteristic of the concave reach and aerator, it is extremely easy to cause low pressure and leads side-walls to be destroyed by cavitation. Experimental results indicate that un-airflow areas and low pressure areas appear on the bottom of concave reach. In paper through model experiment, preventing cavitation damage measures of the Vertical-Bend spillway tunnel side-walls were studied, an aerator with side-walls sudden enlargement and soleplate vertical dropping was introduced on the bottom of concave reach. Experimental results indicate that applying this aerator can effectively eliminate un-airflow areas on the side-walls and increase air entrainment quantity. Observation shows that lateral cavity and bottom cavity are linked each other and water body behind aerator is forced aeration with the whole section. So sidewalls and soleplates are protected. Test results have the model significance to the other similar projects.

KEYWORDS

High head, Free flow spillway tunnel, Sudden enlargement side-walls, Preventing cavitation damage, Hydraulic test

1 INTRODUCTION

With the construction development and increase of the hydroelectric project with the large discharge and high dam, high-speed and ultrafast flow become general. The problems brought by high-speed and ultrafast flow cause great concern for technical staff. Recent project operation practice and model experimental study indicate that forced aeration establishments are generally used for protecting soleplate and the side-walls with high speed flows and low pressure areas tend to be neglected. Especially for Vertical-Bend free flow spillway tunnel behind concave reach side-

walls tend to appear un-airflow areas. Some side-walls were damaged by cavitation, which influenced the safe operation of the building or caused the destruction of the building.

Complexity of mechanism on the basis of cavitation, aerator form of side-walls of closed structure flow is unsatisfied and lateral cavity is difficult to take shape. This paper will combine research results and project experience, clarify cavitation characteristic and cavitation damage mechanism for hydraulic structures with high head. Through model experiment an effective aerator form is to be proposed to protect side-walls and soleplates for Vertical-Bend free flow spillway tunnel.

2 SIDE-WALLS CAVITATION DAMAGE MECHANISM

In the last few years in order to solve cavitation damage of behind segmental sluice gate of bottom outlet with high head, side-walls sudden enlargement and soleplate vertical dropping aerator was adopted at large (Xiao 2000). But because of lacking in perfect project experience and theory basic, side-walls of bottom sluice were destroyed by cavititation in some hydraulic structure (Zhou 1997; Wu 2000; Regan 1990; CHEN 1992).

Areas are prone to be destroyed by cavitation near down-tangential point of concave reach of Vertical-Bend free flow spillway tunnel. Some scholars have done a lot of work about cavitation. Preventing cavitation damage of side-walls was studied primarily (Liu 2000).

The increasing gravity or pressure of water body can quicken rising velocity of air bubble. On the straight slope of concave reach, air bubble rises slow and air bubble is close to slope. However on the bottom of concave reach air bubble has already obviously gone up. On the bottom concave reach pressure is reducing along the slope, the centrifugal force has already tended towards disappearing. Though the mainstream presses close to the slope, the air bubble has already obviously gone up to the adjacent place above water, air concentration of section is very little. Furthermore, because self-aeration of water body is still at developing stage on the bottom concave reach, forced aeration of soleplate spreads fully to fail also, there is some un-airflow areas on the side-walls of concave reach downstream, which tends to cause cavitation damage on the side-walls.

3 EXPERIMENTAL SETUP

Physical model was devised according to some Vertical-Bend free flow spillway tunnel, designed by the similar criterion of the gravity. The length scale is 1 : 30. The model tunnel is made up of water inlet section, Vertical-Bend section and straight slope section, which are shown in Figure 1. The tunnel is city gate form with constant cross section, model typical section size is 43.3 cm×45.0 cm (width×height). The radius of concave reach is 333.33 cm and grade of straight slope is 0.079. Maximum unit-discharge in the model is 1.744 $m^3/s \cdot m$. Maximum velocity on the bottom of concave reach in the model is 7 m/s and Renault numbers is $3.13\times10^5-1.84\times10^6$. So the flow state is in the district of obstruction square, which does not consider the influence of viscidity force.